16 August 2026

Dynamic Metal-Semiconductor Electrical Interfaces in Model Cu|ZnO Hydrogenation Catalyst Structures

Ethan Shi[1,2], Arunavo Chakraborty[1,2], Alexis T. Bell[1,3], Neil K. Razdan[1,3], Shannon W. Boettcher[1,2]

1. Departments of Chemical & Biomolecular Engineering and Chemistry, University of California
2. Energy Technology and Systems Division, Lawrence Berkeley National Laboratory
3. Chemical Sciences Division, Lawrence Berkeley National Laboratory

Abstract

$Cu/ZnO/Al_2O_3$ catalysts are commonly used for methanol synthesis, yet the chemical state of the Cu|ZnO interface remains debated. We probe Cu|ZnO interfacial chemistry by measuring junction electrical characteristics under N_2, CO_2 and gas mixtures from 50 to 250 °C and up to 10 bar(a). The pristine interface behaves as a nonideal rectifying Schottky diode, and H_2 exposure drives a reversible transition toward ohmic behavior, with increased apparent n-type donor density in the ZnO and lower Schottky-barrier height. This result implies the electric potential at the putative active-catalyst interface decreases under reactive conditions. Recovery of rectifying behavior under O_2 and H_2-free N_2 or CO_2 argues against persistent Cu–Zn alloying or oxygen-vacancy formation and supports reversible hydrogen doping of ZnO. CO_2 slows H insertion into ZnO relative to N_2, while water strongly suppresses it. Junction electrical measurements thus inform how such catalytic interfaces evolve under reactive conditions.

Dynamic Metal-Semiconductor Electrical Interfaces in Model Cu|ZnO Hydrogenation Catalyst Structures

Ethan Shi[1,2], Arunavo Chakraborty[1,2], Alexis T. Bell[1,3], Neil K. Razdan[1,3], Shannon W. Boettcher*[1,2]

[1]*Departments of Chemical & Biomolecular Engineering and Chemistry, University of California, Berkeley, CA 94720, United States*

[2]*Energy Technology and Systems Division, Lawrence Berkeley National Laboratory, Berkeley, CA 94720, United States*

[3]*Chemical Sciences Division, Lawrence Berkeley National Laboratory, Berkeley, CA 94720, United States*

*email: boettcher@berkeley.edu

Abstract

$Cu/ZnO/Al_2O_3$ catalysts are commonly used for methanol synthesis, yet the chemical state of the Cu|ZnO interface remains debated. We probe Cu|ZnO interfacial chemistry by measuring junction electrical characteristics under N_2, CO_2 and gas mixtures from 50 to 250 °C and up to 10 bar(a). The pristine interface behaves as a nonideal rectifying Schottky diode, and H_2 exposure drives a reversible transition toward ohmic behavior, with increased apparent n-type donor density in the ZnO and lower Schottky-barrier height. This result implies the electric potential at the putative active-catalyst interface decreases under reactive conditions. Recovery of rectifying behavior under O_2 and H_2-free N_2 or CO_2 argues against persistent Cu–Zn alloying or oxygen-vacancy formation and supports reversible hydrogen doping of ZnO. CO_2 slows H insertion into ZnO relative to N_2, while water strongly suppresses it. Junction electrical measurements thus inform how such catalytic interfaces evolve under reactive conditions.

The hydrogenation of CO_2 into useful fuels and chemicals such as methanol is important for closing the carbon cycle.[1] Among CO_2 reduction and hydrogenation products, methanol stands out as a product already manufactured on commodity scale using oxide-supported Cu nanoparticle catalysts.[2-5] While the substrate CO_2 for these catalytic reactors originates from water-gas-shift reaction of feedstock CO within the same reactor bed, CO_2 has been definitively identified as the carbon source for methanol via ^{14}C radiolabel experiments performed in the 1980s.[6]

Within the set of oxide-supported Cu catalysts, $Cu/ZnO/Al_2O_3$ (CZA) has remained the common CO_2-to-methanol catalyst since being established by Imperial Chemical Industries in 1965. Decades of work devoted to the question of why does CZA offer high methanol activity and selectivity – have produced a variety of, sometimes contradictory, hypotheses for the structure of and chemical interactions within the CZA catalyst.[2,7-14]

The structure of the Cu|ZnO junction under reaction conditions has been variously hypothesized to be a metallic Cu-Zn brass,[9,15] mechanically strained Cu|ZnO,[16] a mixed (Cu_xZn_{1-x}) oxide, Cu supported on an oxygen-vacancy-rich ZnO surface,[17] and mobile ZnO islands forming on Cu nanoparticles.[10] Two observations recur in the CZA literature. First, *operando* IR spectroscopy identifies surface-adsorbed formate as the most-abundant reduced species on CZA, yet the site of formate adsorption – Cu vs CuO vs ZnO – remains contentious.[18] Second, the kinetically limited methanol formation rate from these catalysts has been found to correlate linearly with exposed Cu surface area as inferred from N_2O titration of surface Cu,[19] leading to the hypothesis that Cu/CuO alone is responsible for catalytic turnovers, with ZnO/Al_2O_3 providing a stable support.[2] However, N_2O titration as a method of measuring exclusively surface Cu is contentious since N_2O could also react with reduced metal/metal oxide surface species besides metallic Cu.[20] More recent kinetic experiments comparing $Cu\text{-}ZnO\text{-}Al_2O_3$ and $Cu\text{-}Al_2O_3$ found the addition of ZnO increased the site-normalized methanol formation rate without altering differences in CO_2, H_2 and H_2O reactant orders, suggesting ZnO does not generate unique catalytic sites for methanol synthesis, yet increases the rate and selectivity for methanol relative to CO.[14]

Cu, alongside other platinum-group and coinage metals, has a high work function of 4.4–4.9 eV.[21] ZnO is a wide-bandgap semiconductor (E_g = 3.4 eV), readily *n*-doped by trace impurities.[22] Upon contact, the Cu|ZnO junction forms a Schottky barrier for electrons as the Fermi levels of the Cu and ZnO align (Figure 1). Crucially, these barriers in real metal-semiconductor (M-S) systems are influenced by interfacial junction chemistry. Phenomena such as changes to the metal work function and surface dipoles alter the Schottky barrier, while *n*-dopant density alters the depth and extent of the depletion region in the semiconductor (represented by the region where the bands bend in the Figure 1 diagram).[23,24]

Because these junction parameters set the interfacial electric field that any adsorbate at the Cu|ZnO boundary experiences, they may be directly important in catalysis. Interfacial fields and junction effects have been invoked to explain shifts in binding energy and mechanism at Cu|ZnO

and related metal-oxide interfaces,[4,25] where dipolar intermediates such as bent $CO_2^{\delta-}$ and formate are stabilized or destabilized according to the local field.[26-28]

Determining the Schottky barriers of the Cu|ZnO junction (via current-voltage and capacitance-voltage measurements) under gas environments relevant to CO_2-to-methanol catalysis thus offers an indirect probe to the Cu|ZnO junction. Measuring and explaining the evolution of these Schottky junction parameters under these controlled gas environments is the goal of this work.

Before turning to the data, it is useful to introduce the electrical descriptors used below in the context of possible catalytic systems. Each parameter relates in part to the strength of the interfacial field and to how readily electrons cross the Cu|ZnO contact. A rectifying junction passes current in one direction only; it signifies a Schottky barrier which is associated with a substantial interface electric potential step and a depletion region at the interface without mobile electrons in the semiconductor. An ohmic junction passes current in both directions equally well; it signifies either a lack of band bending and thus a small interfacial electric field, or, in cases where the n-type doping of the semiconductor is very high (leading to a very thin depletion region), a charge transfer mechanism based on electron tunneling. A leaky junction is intermediate: some parts of the interface may have rectifying behavior while other parts may have different degrees of ohmic behavior that partially short-circuits the electronic barrier. Because it is the barrier and its associated field that couple to adsorbate dipoles and govern charge transfer at the Cu|ZnO perimeter, a rectifying-to-ohmic transition is, potentially, a useful readout that the electrostatic environment of the putative active interface has changed. That transition, and its reversibility, is what the following experiments measure and which we analyze in the discussion.

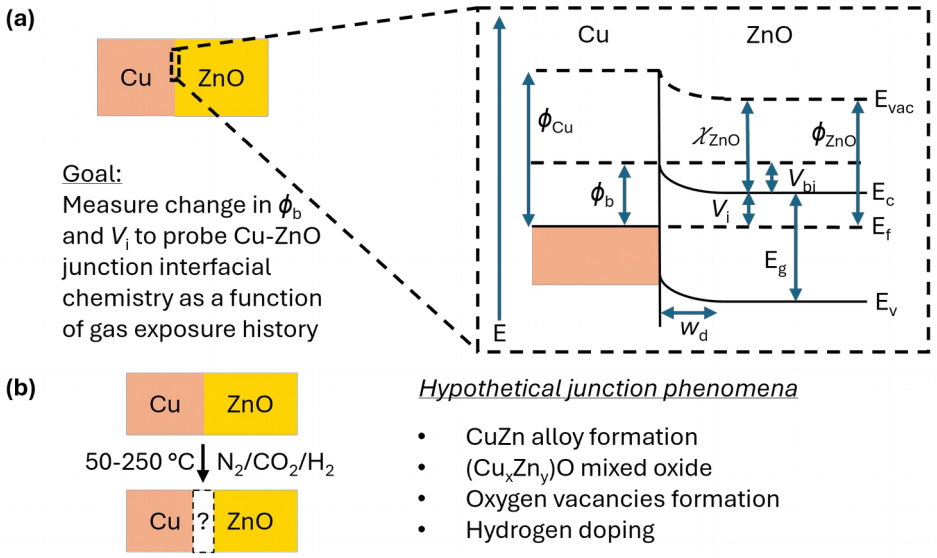

Figure 1. Probing interfacial chemistry of the Cu|ZnO junction by measuring the Schottky junction characteristics. (a) Fermi-level alignment and band-bending at an *ideal* Cu|ZnO junction that results in a Schottky junction. The key junction parameters are: ϕ_{Cu}: Cu work function, ϕ_{ZnO}: ZnO work function, ϕ_b: barrier height, χ_{ZnO}: ZnO electron affinity, V_{bi}: built-in potential, E_g: bandgap, E_{vac}: vacuum level energy, E_c: conduction band energy, E_v: valence

band energy, E_f: Fermi level energy, w_d: depletion width. (b) Hypothetical changes in the Cu|ZnO interface upon controlled gas exposure ($CO_2/H_2/N_2$) at 50–250 °C.

We fabricated Cu|ZnO devices via e-beam evaporation of an array of disc-shaped Cu thin films onto a polished Zn-polar (0001) ZnO single crystal. Thermal evaporation of a Ti|Pt layer on the back of ZnO was used to form an ohmic contact to the entire ZnO crystal. We contacted the Cu spots and Ti back-contact on these devices using electrical feedthroughs to a custom gas-tight chamber with gas inlet and outlet ports. These fixtures facilitated measurement of the electrical characteristics of the Cu|ZnO junction at gas pressures up to 10 bar(a) and temperatures up to 250 °C (details in SI).

The current density-voltage bias (*j*-*V*) measurements of the Cu|ZnO junction under ambient N_2 (25 °C, 1 bar(a)) verify the expected rectifying Schottky junction (Figure 2). We ascribe the linear *j*-*V* dependence at large forward bias voltage (0.3–0.5 V) to the sum of ohmic drops through the contact probes, the bulk Cu, the bulk ZnO, Ti and Pt. Subtracting the ohmic loss from the applied junction potential (**Figure S2**), we obtain the *j*-*V* characteristics of the Cu|ZnO junction that obey the Shockley diode equation

$$j = j_s\left(e^{\frac{qV}{nk_bT}} - 1\right) \qquad \text{(Eqn. 1)}$$

where j_s is the reverse-bias saturation current, q is the magnitude of elementary charge, k_b is the Boltzmann constant, T is the temperature and n is the diode ideality factor. At forward-bias significantly greater than the thermal voltage V_T ($V_T = \frac{k_bT}{q}$¿, the *j*-*V* approximates to the following expressions.

$$j \approx j_s e^{\frac{qV}{nk_bT}} \qquad \text{(Eqn. 2)}$$

$$\ln(j) \approx \ln(j_s) + \frac{q}{nk_bT}V \text{ (Eqn. 3)}$$

The reverse-bias saturation current j_s originates from thermionic injection of charge carriers to the ZnO conduction band and thus depends on temperature and the Schottky junction barrier height ϕ_b, as described in the Richardson equation

$$j_s = A^{¿}¿ \qquad \text{(Eqn. 4)}$$

where j_s is the reverse-bias saturation current, $A^{¿*¿¿}$is the Richardson constant, q is the magnitude of elementary charge, k_b is the Boltzmann constant, T is the temperature and ϕ_b is the Schottky barrier height. Because j_s depends exponentially on ϕ_b, the junction current is a sensitive probe of the interface. At 70 °C, where k_bT/q ≈ 30 mV, a 60 meV change in barrier height alters the current eightfold. This makes the barrier height a practical quantity to track in supported-metal catalysts, where the oxide support is often a semiconductor.

The Schottky barrier of an *ideal* M-S junction is the difference between the metal work function (in this case, ϕ_{Cu}) and the electron affinity of the semiconductor (χ_{ZnO}, the energy difference between the conduction band and vacuum energy).

$$\phi_b^{ideal} = \phi_{Cu} - \chi_{ZnO} \qquad \text{(Eqn. 5)}$$

Both metal work function and semiconductor electron affinity are facet dependent. The ideal Schottky barrier for a Cu(111)|ZnO(0001) junction is near 1.0 eV (ϕ_{Cu} = 4.9 eV, χ_{ZnO} = 3.9 eV for this surface).

The Schottky barrier in real M-S junctions is modified by the presence of surface dipoles, impurities and dopants at the M-S interface, all collected into an interfacial $\Delta_{\int ¿¿}$ energy term. The value of ϕ_b^{real} may be important for supported metal catalyst systems because it is related to the amount of interfacial charge transfer and interfacial electric fields at equilibrium.

$$\phi_b^{real} = \phi_{Cu} - \chi_{ZnO} + \Delta_{\int ¿¿} \text{ (Eqn. 6)}$$

Furthermore, a polycrystalline M-S interface can be spatially heterogeneous, with several pairs of metal and semiconductor facets at a real junction – the lowest local Schottky barrier would dominate the results of *j*-*V* measurements in these cases.

At room temperature, we measured the Schottky barrier $\phi_{b,JV}$ of the Cu|ZnO junction to be 0.40–0.50 eV. We also determined the diode ideality factor *n* for the Cu|ZnO devices to be 1.6–1.8, consistent with a non-ideal diode where only a fraction of the junction voltage contributes to altering the thermionic injection of carriers into the ZnO conduction band.

The non-ideality of the Cu|ZnO junction extends to its reverse-bias behavior, with the current magnitude increasing linearly with the applied reverse-bias voltage, instead of converging to the reverse-bias saturation current. We model this behavior with an explicit junction shunt resistance R_{shunt} as a descriptor of the electrical non-ideality of this Schottky junction. The total current through the Cu|ZnO junction is

$$j = j_{Schottky} + j_{shunt} \quad \text{(Eqn. 7)}$$

$$j_{Schottky} = j_s\left(e^{\frac{qV_{Cu-ZnO}}{nk_bT}} - 1\right) \qquad \text{(Eqn. 8)}$$

$$j_{shunt} = \frac{V_{Cu-ZnO}}{R_{shunt}} \quad \text{(Eqn. 9)}$$

At large negative junction bias, the slope of the j-$V_{\text{Cu|ZnO}}$ converges to $1/R_{shunt}$. We subtract j_{shunt} from the measured current density to isolate the Schottky junction current.[29,30]

Beyond junction *j*-*V* measurements, AC electrical impedance measurements helped establish the differential capacitance of the Cu|ZnO junction held at varying reverse-bias potentials. The ZnO

depletion layer proximate to the Cu|ZnO interface behaves as a uniformly charged dielectric, with the layer thickness depending on the applied (reverse-bias) voltage across the junction. The inverse square of the junction differential capacitance is then found to depend linearly on the reverse-bias junction voltage as illustrated in the Mott-Schottky equation

$$\frac{1}{C_{diff}^2(V)} = \frac{2}{\varepsilon_r \varepsilon_0 A^2 q N_D}\left(V_{bi} - V - \frac{k_b T}{q}\right) \quad \text{(Eqn. 10)}$$

where C_{diff} is the differential capacitance, ε_0 is the vacuum permittivity, ε_r is the semiconductor dielectric constant (ε_{ZnO} = 8.0) [31], A is the junction area, V is the potential applied to the Cu contact relative to the ZnO ohmic contact (with reverse bias taken as negative), q is the magnitude of elementary charge, k_b is the Boltzmann constant, T is the temperature, V_{bi} is the band-bending potential between the bulk ZnO conduction band and the ZnO conduction band at the Cu|ZnO interface, and N_D is the dopant density.

We determined the dopant density of the ZnO from Mott-Schottky measurements of the Cu|ZnO junction to be 10^{14}–10^{16} cm^{-3} (**Figure S2**) and a ZnO conduction band bending (built-in potential, V_{bi}) between the Cu|ZnO junction and the bulk ZnO to be 0.6–0.9 eV. The dopant density is consistent with typical *n*-doping of hydrothermally synthesized ZnO single crystals[22] and corresponds to a bulk ZnO Fermi-level - conduction band energy separation ~ 0.15 eV. The Schottky barrier from capacitance-voltage measurement is thus inferred to be 0.75–1.05 eV, referred to hereafter as $\phi_{b,CV}$.

The ZnO depletion width under zero external bias is given by

$$W_0 = \sqrt{\frac{2\varepsilon_0 \varepsilon_r V_{bi}}{q N_D}} \quad \text{(Eqn. 11)}$$

where ε_0 is the vacuum permittivity, ε_r is the semiconductor dielectric constant, q is the magnitude of elementary charge, k_b is the Boltzmann constant, T is the temperature, V_{bi} is the band-bending potential between the bulk ZnO conduction band and the ZnO conduction band at the Cu|ZnO interface, and N_D is the dopant density. We estimate the zero-bias depletion-layer thickness of 80-200 nm.

These ambient *j*-*V* and C_{diff}-*V* measurements of the Cu|ZnO junction establish a non-ideal spatially heterogeneous Cu|ZnO Schottky junction with a benchmark Schottky barrier ($\phi_{b,JV}$ = 0.4–0.5 eV and $\phi_{b,CV}$ = 0.75–1.05 eV), a bulk ZnO *n*-dopant density of 10^{14}–10^{16} cm^{-3}, alongside methodologies to measure chemically induced changes to the Cu|ZnO junction.

We emphasize the difference in the Schottky barrier height from j-V measurements and junction capacitance measurements supports the spatial heterogeneity of the Schottky barrier across the Cu|ZnO junction.[23] The j-V measurements reflect the lower range of the distribution of barriers across the full junction since these regions carry the majority of the total current passed through

the junction. Mott-Schottky analysis offers a weighted average of the Schottky barrier height since the depletion layer differential capacitance is measured across the entire junction, including regions with a high local Schottky barrier height that would not carry significant current density during *j*-*V* measurements.

The Cu|ZnO junction remains rectifying when heated under ambient pressure N_2 or CO_2, with increasing reverse-bias current with increasing temperature (**Figure 2a**), with no irreversible changes upon thermal cycling – the Schottky barrier of 0.42 eV and dopant density ~ 4×10^{16} cm^{-3} persist. The Cu|ZnO junction becomes ohmic and remains ohmic when heated to 250 °C with 20% H_2 (diluted in N_2 or CO_2) and cooled to room temperature under the same atmosphere (**Figure 2b** and **Figure S3**). If stored at room temperature under an inert N_2 atmosphere, the junction remains ohmic while returning to a rectifying Schottky junction if exposed to air (on a ~24-h timescale, Figure 2d-e). Finally, the Cu|ZnO junction returns to a rectifying Schottky junction if heated under a H_2-free CO_2 or N_2 atmosphere (**Figure 2c**).

The reversible conversion of the Cu|ZnO junction between ohmic and Schottky behavior provides evidence against persistent bulk Cu–Zn alloying as the dominant origin of the electrical change, although single-atom or atomic-layer Cu-Zn alloying could still be plausible.[32] The H_2-exposed Cu|ZnO junction converting to rectifying upon air exposure at room temperature is consistent with both H- and oxygen-vacancy based doping of ZnO (doubly positively charged, denoted as $V_O^{\cdot\cdot}$ in the Kröger-Vink notation).

For oxygen-vacancy based doping: $H_2(g)+O_O^{\times}\rightleftharpoons V_O^{\cdot\cdot}+H_2O(g)+2e'$

For interstitial H atom doping: $\frac{1}{2}H_2(g)\rightleftharpoons H_i^{\cdot}+e'$

The return of rectification upon heating under N_2 *in the absence of air* is consistent with H doping of ZnO rather than O vacancy formation, as there is no oxygen source present in the system to fill the vacancies. Thus, air exposure likely provides a stronger thermodynamic driving force for the removal of mobile dopant H from the ZnO, generating trace water vapor as a product, instead of surface H—H recombination under air-free conditions.

H de-doping in the absence of O_2: $H_i^{\cdot}+e'\rightleftharpoons\frac{1}{2}H_2(g)$

H de-doping in the presence of O_2: $\frac{1}{2}O_2+2H_i^{\cdot}+2e'\rightleftharpoons H_2O(g)$

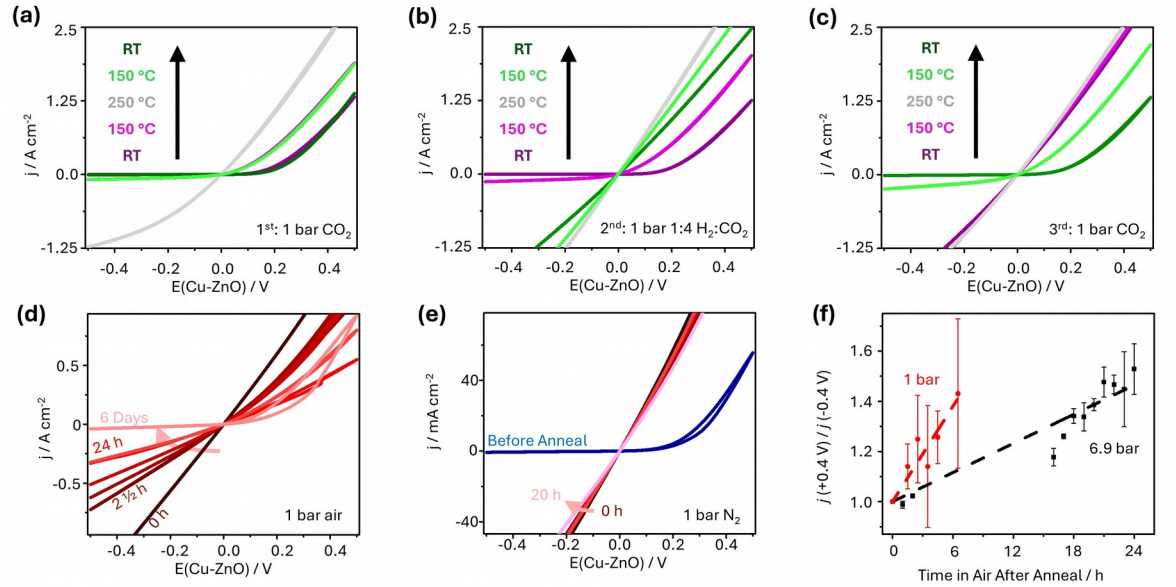

Figure 2. ZnO junction *n*-doping by H_2 exposure converts from the rectifying Cu|ZnO Schottky junction to an ohmic junction. In-situ *j-V* measurements of a representative Cu|ZnO junction at 50 °C intervals between RT and 250 °C in 0% H_2 (a), 20% H_2 (b) and 0% H_2 (c), diluted in CO_2 demonstrate thermally reversible *n*-doping by H up to degenerate dopant density (>10^{19} cm^{-3}). The ohmic H-doped Cu|ZnO junction recovers to a Schottky barrier at room temperature when exposed to air (d) but persists if stored under N_2 (e). H doping with high pressure H_2 results in an ohmic junction that is slower in recovering a Schottky barrier (f).

Furthermore, oxygen-vacancy-related states in ZnO are generally deep donors, approximately 1.0 eV below the conduction-band edge, which means they do not contribute much to the free electron concentration in the conduction band.[33] Oxygen vacancy concentration (measured via photoluminescence and EPR) in ZnO samples is also known to increase upon being heated in an inert O_2-free N_2/Ar atmosphere,[34] contrary to our observations of Cu|ZnO Schottky barrier recovery upon heating in N_2.

We note prior work on metal oxides by Frost and coworkers in 1988 [25] invokes formation of O-vacancies and the Schottky junction for catalytic methanol synthesis on Cu/ThO_2 using CO as the feedstock but no direct junction electrical measurements were reported. CO as a stronger reductant than H_2 could also generate O-vacancies in the ZnO where H_2 does not. Claims of O vacancies on ZnO and other oxides upon H_2 exposure supported with XPS measurements tend to be erroneous, with changes to O1s spectra originating from surface metal hydroxides.[35-39] We note that similar results have been found for Pd|ZnO Schottky diodes in the context of H_2 gas sensors.[40] In our case, Cu|ZnO devices annealed at 250 °C with greater H_2 partial pressure (4 bar(a)) return to a rectifying Schottky junction on a longer timescale, consistent with H doping of ZnO to a greater depth under the Cu|ZnO junction (**Figure 2f**).

We deliberately performed subsequent measurements with junctions held at 70 °C to slow the doping of the ZnO seen at >200 °C so we could capture changes in the Cu|ZnO junction barrier height, dopant density, etc.

We found exposure to pressurized H_2 (p_{H_2} = 2.75 bar(a)) is essential to doping the Cu|ZnO junction at 70 °C – low pressure H_2 exposure (p_{H_2} = 0.5 bar(a)) does not convert the Cu|ZnO junction into an ohmic junction (**Figure S5**). We describe the conversion of the Schottky junction to an ohmic junction using the Cu|ZnO junction shunt resistance, described previously. At p_{H_2}= 2.75 bar(a), the junction becomes ohmic within 1 h while remaining a leaky Schottky junction for p_{H_2}= 0.5 bar(a). We further note that doping the Cu|ZnO junction from H_2 diluted in CO_2 was found to be slower than H_2 diluted in N_2 for the same H_2 partial pressure (Figure 3).

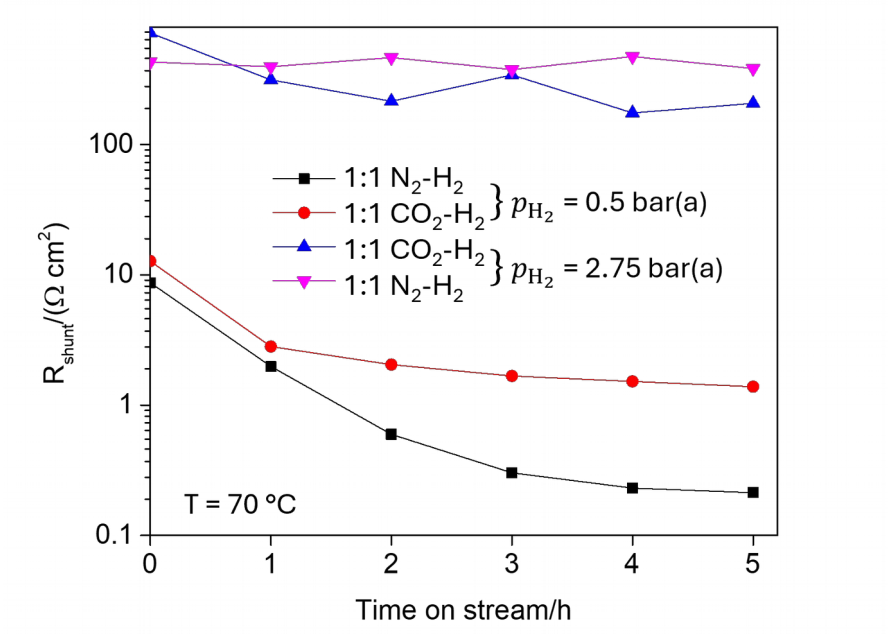

Figure 3. CO_2 as a diluent for H_2 gas inhibits H doping of ZnO relative to an inert gas (N_2). The junction shunt resistance determined from *j-V* measurements of the Cu|ZnO junction describes the transition of the junction from a rectifying Schottky junction to an ohmic junction. Typical series resistance extracted from forward bias data ranges from 0.1–1 Ω.

The surface adsorption and diffusion of H atoms in ZnO at varying temperatures have been previously explored on single-crystal ZnO samples under ultra-high vacuum conditions, using plasma and thermally dissociated H atoms. [41,42] We estimate the diffusion coefficient of the H in ZnO from these prior reports $D_H = 1.2 \times 10^{-10}\ cm^2\ s^{-1}$ (¿ $1.2 \times 10^{-2}\ \mu m^2\ s^{-1}$) at 70 °C. Assuming 1D diffusion of H atoms into the ZnO, the characteristic distance at which the concentration of the diffusing species reaches 16% of the concentration at the source (i.e. the diffusion length $L = 2\sqrt{(D_H t)}$, the depth at which the error-function (erfc) solution to Fick's second law falls to erfc(1) ≈ 0.16 of the source concentration), for H diffusion reaches a 100 nm depth in ~0.2 s, and a 1 μm depth in 21 s.

$$t = \frac{L^2}{4 D_H}$$

Combined with the approximate threshold for degenerate dopant density of 10^{19} cm^{-3} (i.e. *n*-doping density where the ZnO conduction band-Fermi level gap becomes comparable to thermal voltage and the Cu|ZnO junction ceases to be a Schottky barrier), bulk H diffusion into the ZnO is unlikely to limit the rate of H_2-driven H-doping of the ZnO. H adsorption on the ZnO surface, and the transport of surface H to bulk H become the likely processes to govern the overall rate of ZnO *n*-doping by H_2.

We next looked at the impact of three typical CZA catalyst poisons – alkanethiols, dichloromethane and water vapor – on H_2-gas-driven H-doping of the Cu|ZnO junction. Two of these – the thiol and the DCM – were chosen as chemically selective toward the Cu surface. Octadecanethiol emulates the strong adsorption of H_2S on metal surfaces and forms a self-assembled monolayer on copper surfaces,[43] while DCM chlorinates the surface-accessible Cu to make a layer of CuCl.[12] Water vapor is not expected to have a simple Cu-vs-ZnO site selectivity, with a more complex catalyst poisoning mechanism.[14]

C_{18}-SH SAMs were grown by immersing the Cu|ZnO single crystal devices in a 10 mM C_{18}-SH solution in toluene for 12 h. The formation of the SAM was verified by contact angle measurements (**Figure S4**). These thiol-coated devices were exposed to a maximum temperature of 70 °C to avoid damage to the thiol SAM, and the presence of the SAM was verified by contact angle measurement after thermal cycling. Upon H_2 exposure at 70 °C (p_{H_2} = 0.5 bar(a)), the barrier height $\phi_{b,JV}$ decreases while the dopant density N_D increases, just as with the untreated Cu|ZnO junction (**Figure 4b**).

Similarly, the Cu|ZnO junction was pre-treated with DCM vapor (p_{DCM} = 0.13 kPa) in N_2 at 200 °C for 1 h. Surface Cu is known to react and form CuCl under these conditions.[12] We found H_2-driven H doping on the DCM-treated Cu|ZnO device also continued with large losses to the apparent $\phi_{b,JV}$.

Exposure to water, introduced to the measurement chamber via a stream of 1:1 N_2-H_2 humidified through water held at 40 °C (p_{H_2O} = 7.3 kPa), was far more significant in arresting H-doping of the ZnO as shown by lack of significant changes in both ϕ_b and N_d when humidity was present (**Figure 4b**).

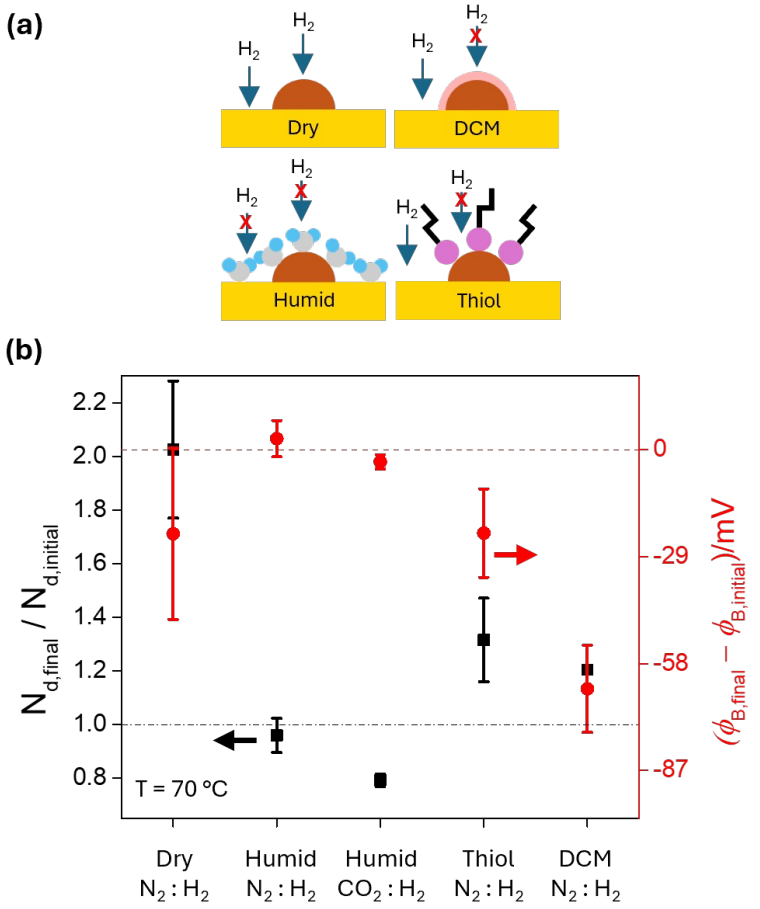

Figure 4. Water vapor, but not thiol or DCM surface treatment, suppresses H-doping of ZnO. (a) Cu|ZnO junction devices were exposed to DCM, octadecanethiol and water vapor. Junctions were exposed to DCM and octadecanethiol *ex-situ*, while water vapor was co-fed with H_2 diluted in N_2 or CO_2 (p_{H_2} = 0.5 bar(a), p_{H_2O} = 7.3 kPa). (b) Change in ZnO dopant density and in Schottky barrier height for each surface-modified sample after 7 h of exposure to the respective diluted H_2 gas stream at 70 °C. Black symbols (left axis) give $N_{d,final}/N_{d,initial}$, the ratio of the dopant density determined by Mott-Schottky analysis after exposure to that determined on the same device before exposure; a ratio of one (dash-dot line) indicates no net doping change. Blue symbols (right axis) give $\varphi_{B,final} - \varphi_{B,initial}$, the corresponding change in the *j-V* Schottky barrier height in volts; a value of 0 (dotted line) indicates no change in barrier height. Dopant density is unaltered or decreases under humid H_2 in both N_2 and CO_2 diluents, whereas the dry, thiol-treated and DCM-treated junctions all show net *n*-doping accompanied by a loss in barrier height.

We measured the *n*-doping of ZnO upon exposure to CO_2, N_2 and H_2 gas at 50–200 °C and found the changes to the junction electronic properties to be most consistent with *n*-doping of the ZnO by H_2 dissociation and H diffusion into the ZnO. H is a shallow *n*-donor (i.e. that easily thermally generates free electrons) for ZnO.[44] The *j-V* data is inconsistent with bulk Cu-Zn alloying, which would not be expected to be reversible. We estimate the diffusion coefficient of Zn metal in Cu-Zn brass from prior ^{65}Zn radiotracer measurements to be $D_{Zn} = 7.0 \times 10^{-2}\,\text{Å}^2\,s^{-1}$ at 250 °C and $3.1 \times 10^{-15}\,\text{Å}^2\,s^{-1}$ at 20 °C.[45] Assuming 1D diffusion of Zn metal from the Cu|ZnO junction into the Cu metal, we calculate the characteristic diffusion length L_{Zn} ~ 15.6 nm over 24 h. Upon cooling to room temperature, this inter-diffused Zn in Cu would be effectively frozen, with

characteristic diffusion length for back-diffusion ~ 3.3×10^{-6}nm over 24 h. Recovery of Schottky diode junction on 24-h timescale thus renders bulk Cu-Zn alloy formation unlikely.

Recovery of degenerate-doped ohmic Cu|ZnO junctions to a rectifying Schottky junction upon annealing at >200 °C under N_2 and CO_2 without O_2 exposure is also inconsistent with oxygen vacancies being the dopant. H_2 exposure at 250 °C led to rapid degenerate ZnO *n*-doping, so junction *j*-*V* and capacitance measurements at 70 °C were performed to resolve changes to the Schottky barrier height and dopant density. Co-feeding H_2 with CO_2 led to slower H doping than when N_2 was co-fed with H_2 to the Cu|ZnO junction, presumably due to slower H_2 dissociation and/or H insertion kinetics when CO_2 was adsorbed on the surface. Among the three CZA poisons introduced to the Cu|ZnO junction, water vapor inhibited ZnO H doping, while junction treatment with C_{18}-SH and CH_2Cl_2, both intended to block H adsorption on Cu, had much less impact on H doping of the ZnO.

While the increase in dopant density in ZnO is readily explained by H doping, the precise chemical origin of the change in the Cu|ZnO barrier height is more difficult to assign. Adsorbed H is known to lower the work function of Pt(111), by ~0.23 eV,[46] and hydrogen-induced changes in metal work function or interfacial dipole have been invoked to explain the loss of rectification and apparent Schottky-barrier lowering of Pt/ZnO[47] and Pd/ZnO[48] hydrogen sensors. Given the high diffusivity of H in ZnO,[42] [41] dissociated H is likely to be present at the Cu|ZnO interface under H_2 fed conditions. Such interfacial H very likely modifies the Cu|ZnO energy-level alignment through a change in the interfacial dipole, thereby lowering the Schottky barrier. For example, hydrogenation could transform an initially O-rich Cu–O–Zn interfacial motif into a Cu–H···HO–Zn configuration or related hydrogenated structure. Proving the presence of interfacial H is difficult and beyond the scope of this study. Recent work by Christensen and coworkers, however, measured H uptake by Cu-ZnO-Al_2O_3 treated under H_2 atmosphere and found substantial H absorption (up to 0.0407 mol_H/mol_{ZnO}), scaling linearly with the surface area of Cu-ZnO interface across ZnO, Cu-ZnO and Cu-ZnO-Al_2O_3.[49]

While noting the strong diagnostic inferences drawn from these junction electrical measurements at the model Cu|ZnO(0001) junction, we did not measure the rate of CO_2 hydrogenation catalyzed by this macroscopic Cu|ZnO junction as it lacks the requisite surface area to produce methanol or CO that would be measurable with a typical gas chromatograph.

We note the typical activation of CZA catalysts involves reduction of a CuO-ZnO-Al_2O_3 composite under a H_2 stream to yield Cu nanoparticles. The resulting ZnO could be *n*-doped by Al, and *p*-doped by Cu. Combined with high water, CO_2, CO and H_2 partial pressures, it is not immediately evident if the Cu|ZnO junction for an operating catalyst would possess a Schottky barrier. We note recent use of microwave cavity perturbation technique (MCPT) to measure the microwave absorption-dissipation-reflection by a CZA pellet in CO_2-H_2 atmospheres at 230 °C.[50] The sample effective dielectric constant decreased upon activation (reduction under H_2) of Cu-ZnO-Al_2O_3. Subsequent cyclic exposure of the CZA pellet to gas feeds with high CO_2

concentration increased the sample effective dielectric constant, while greater H_2 concentration lowered the apparent dielectric constant, consistent with H-doping of the ZnO increasing the bulk electron conductivity and lowering particle-particle resistances. This previous work is thus consistent with our own data and interpretation indicating both H insertion into ZnO and doping, and a lowering of the interfacial barrier height with Cu.

Probing the electrical characteristics of a Cu|ZnO system with an interpenetrating porous Cu|ZnO network could enable simultaneous measurement of CO_2 hydrogenation products and would be desirable to correlate changes to junction characteristics to relevant changes to catalysis. Analysis of porous junctions, however, would be far more complex due to junction heterogeneity and ambiguous interfacial area. This work with the simple model Cu|ZnO single-crystal junction helps build towards that more complex experiment by establishing methods and benchmarking the Cu|ZnO junction under controlled gas environments at 50-250 °C.

More broadly, ideas around Schottky junctions being catalytic sites for thermocatalytic reactions, and the notion of tuning catalysis rates and selectivity via controlled junction bias have existed since at least the 1980s. Electrical monitoring of catalyst state during gas-phase turnover has precedent in catalytic-gate metal-oxide-semiconductor (MOS) and metal-insulator-semiconductor (MIS) devices.[51] In early Pd–MOS studies, reaction-induced capacitance–voltage shifts were used to monitor hydrogen populations during Pd-catalyzed H_2 oxidation, while later catalytic-gate SiC devices related current–voltage or capacitance–voltage changes to reactions occurring in CO-, hydrocarbon-, NH_3-, and O_2-containing gas mixtures.[52] In these devices and similar devices looking at chemical reaction induced electrical current (chemicurrent) by the McFarland and Somorjai groups, [53-67] however, the electrical response primarily transduced adsorbate-induced work-function or buried-interface dipole changes. *Operando* extraction of the transport parameters of a directly exposed catalyst–support metal|semiconductor junction, coupled to simultaneous product analysis, remains largely unexplored.

Corresponding Author

Shannon W. Boettcher – Departments of Chemical & Biomolecular Engineering and Chemistry, University of California, Berkeley, CA 94720, USA; Energy Technology and Systems Division, Lawrence Berkeley National Laboratory, Berkeley, CA 94720, USA; Email: boettcher@berkeley.edu

Author Contributions

E.S. and S.W.B. conceptualized and led the project. E.S. conducted experiments, engineered custom cells, and analyzed data. S.W.B. and A.C. provided feedback on experiments and data analysis. All authors contributed to writing and provided feedback on the manuscript.

Notes

The authors declare no competing financial interest.

Data Availability Statement

The data underlying this study are available in the published article and its Supporting Information.

Acknowledgements

This work was supported by the Division of Chemical Sciences, Geosciences, and Biosciences of the U.S. Department of Energy at LBNL under Contract No. DE-AC02-05CH11231 as a part of the Catalysis and Chemical Transformations Program. This work used shared instrumentation at Lawrence Berkeley National Laboratory.

Supporting Information

The Supporting Information is available free of charge at https://pubs.acs.org/doi/10.1021/acs.jpclett.XXXXXXX.

Experimental procedures for device fabrication, testing and data analysis; supplementary current–voltage and capacitance–voltage data (PDF).

References

(1) Shaw, W. J.; Kidder, M. K.; Bare, S. R.; Delferro, M.; Morris, J. R.; Toma, F. M.; Senanayake, S. D.; Autrey, T.; Biddinger, E. J.; Boettcher, S.; et al. A US Perspective on Closing the Carbon Cycle to Defossilize Difficult-to-Electrify Segments of Our Economy. *Nat. Rev. Chem.* **2024**, *8* (5), 376-400. DOI: 10.1038/s41570-024-00587-1.

(2) Beck, A.; Newton, M. A.; van de Water, L. G. A.; van Bokhoven, J. A. The Enigma of Methanol Synthesis by Cu/ZnO/Al_2O_3-Based Catalysts. *Chem. Rev.* **2024**, *124* (8), 4543-4678. DOI: 10.1021/acs.chemrev.3c00148.

(3) Ye, R.-P.; Ding, J.; Gong, W.; Argyle, M. D.; Zhong, Q.; Wang, Y.; Russell, C. K.; Xu, Z.; Russell, A. G.; Li, Q.; et al. CO_2 hydrogenation to high-value products via heterogeneous catalysis. *Nat. Commun.* **2019**, *10* (1), 5698. DOI: 10.1038/s41467-019-13638-9.

(4) Kattel, S.; Liu, P.; Chen, J. G. Tuning Selectivity of CO_2 Hydrogenation Reactions at the Metal/Oxide Interface. *J. Am. Chem. Soc.* **2017**, *139* (29), 9739-9754. DOI: 10.1021/jacs.7b05362.

(5) Taheri Najafabadi, A. CO_2 Chemical Conversion to Useful Products: An Engineering Insight to the Latest Advances Toward Sustainability. *Int. J. Energy Res.* **2013**, *37* (6), 485-499. DOI: 10.1002/er.3021.

(6) Chinchen, G. C.; Denny, P. J.; Jennings, J. R.; Spencer, M. S.; Waugh, K. C. Synthesis of Methanol: Part 1. Catalysts and Kinetics. *Appl. Catal.* **1988**, *36*, 1-65. DOI: 10.1016/S0166-9834(00)80103-7.

(7) Bando, K. K.; Sayama, K.; Kusama, H.; Okabe, K.; Arakawa, H. In-situ FT-IR Study on CO_2 Hydrogenation over Cu Catalysts Supported on SiO_2, Al2O_3, and TiO_2. *Appl. Catal., A* **1997**, *165* (1), 391-409. DOI: 10.1016/S0926-860X(97)00221-4.

(8) Hu, J.; Li, Y.; Zhen, Y.; Chen, M.; Wan, H. In Situ FTIR and Ex Situ XPS/HS-LEIS Study of Supported Cu/Al_2O_3 and Cu/ZnO Catalysts for CO_2 Hydrogenation. *Chin. J. Catal.* **2021**, *42* (3), 367-375. DOI: 10.1016/s1872-2067(20)63672-5.

(9) Van Herwijnen, T.; De Jong, W. A. Brass Formation in a Copper/Zinc Oxide CO Shift Catalyst. *J. Catal.* **1974**, *34* (2), 209-214. DOI: 10.1016/0021-9517(74)90030-X.

(10) Behrens, M.; Studt, F.; Kasatkin, I.; Kühl, S.; Hävecker, M.; Abild-Pedersen, F.; Zander, S.; Girgsdies, F.; Kurr, P.; Kniep, B.-L.; et al. The Active Site of Methanol Synthesis over Cu/ZnO/Al_2O_3 Industrial Catalysts. *Science* **2012**, *336* (6083), 893-897. DOI: 10.1126/science.1219831.

(11) Frei, E.; Gaur, A.; Lichtenberg, H.; Zwiener, L.; Scherzer, M.; Girgsdies, F.; Lunkenbein, T.; Schlögl, R. Cu−Zn Alloy Formation as Unfavored State for Efficient Methanol Catalysts. *ChemCatChem* **2020**, *12* (16), 4029-4033. DOI: 10.1002/cctc.202000777.

(12) Lin, T. C.; Bhan, A. Rates and Reversibility of CO_2 Hydrogenation on Cu-based Catalysts. *J. Catal.* **2024**, *429*, 115214. DOI: 10.1016/j.jcat.2023.115214.

(13) Kunkes, E. L.; Studt, F.; Abild-Pedersen, F.; Schlögl, R.; Behrens, M. Hydrogenation of CO_2 to Methanol and CO on Cu/ZnO/Al_2O_3: Is There a Common Intermediate or Not? *J. Catal.* **2015**, *328*, 43-48. DOI: 10.1016/j.jcat.2014.12.016.

(14) Lin, T. C.; Nolen, M. A.; Farberow, C. A.; Kwon, S.; Bhan, A. Mechanistic and Kinetic Relevance of Hydrogen and Water in CO_2 Hydrogenation on Cu-Based Catalysts. *J. Catal.* **2025**, *443*, 115936. DOI: 10.1016/j.jcat.2024.115936.

(15) Spencer, M. S. α-brass Formation in Copper/Zinc Oxide Catalysts: II. Diffusion of Zinc in Copper and α-brass under Reaction Conditions. *Surf. Sci.* **1987**, *192* (2), 329-335. DOI: 10.1016/S0039-6028(87)81128-7.

(16) Kasatkin, I.; Kurr, P.; Kniep, B.; Trunschke, A.; Schlögl, R. Role of Lattice Strain and Defects in Copper Particles on the Activity of $Cu/ZnO/Al_2O_3$ Catalysts for Methanol Synthesis. *Angew. Chem., Int. Ed.* **2007**, *46* (38), 7324-7327. DOI: 10.1002/anie.200702600.

(17) Zhang, F.; Li, B.; Quan, X.; Wang, K.; Xu, J.; Wu, T.; Li, Z.; Yan, M.; Liu, S.; He, Y.; et al. Revealing the Dynamics of Oxygen Vacancy in ZnO_{1-x}/Cu during Robust Methanol Synthesis from CO_2. *ACS Catal.* **2024**, *14* (9), 7136-7148. DOI: 10.1021/acscatal.4c01648.

(18) Tarasov, A. V.; Seitz, F.; Schlögl, R.; Frei, E. In Situ Quantification of Reaction Adsorbates in Low-Temperature Methanol Synthesis on a High-Performance Cu/ZnO:Al Catalyst. *ACS Catal.* **2019**, *9* (6), 5537-5544. DOI: 10.1021/acscatal.9b01241.

(19) Zhang, H.; Chen, J.; Han, X.; Pan, Y.; Hao, Z.; Tang, S.; Zi, X.; Zhang, Z.; Gao, P.; Li, M.; et al. High-Performance $Cu/ZnO/Al_2O_3$ Catalysts for CO_2 Hydrogenation to Methanol. *Ind. Eng. Chem. Res.* **2024**, *63* (14), 6210-6221. DOI: 10.1021/acs.iecr.4c00357.

(20) Fichtl, M. B.; Schumann, J.; Kasatkin, I.; Jacobsen, N.; Behrens, M.; Schlögl, R.; Muhler, M.; Hinrichsen, O. Counting of Oxygen Defects versus Metal Surface Sites in Methanol Synthesis Catalysts by Different Probe Molecules. *Angew. Chem., Int. Ed.* **2014**, *53* (27), 7043-7047. DOI: 10.1002/anie.201400575.

(21) Derry, G. N.; Kern, M. E.; Worth, E. H. Recommended Values of Clean Metal Surface Work Functions. *J. Vac. Sci. Technol., A* **2015**, *33* (6), 060801. DOI: 10.1116/1.4934685.

(22) Janotti, A.; Van de Walle, C. G. Fundamentals of Zinc Oxide as a Semiconductor. *Rep. Prog. Phys.* **2009**, *72* (12), 126501. DOI: 10.1088/0034-4885/72/12/126501.

(23) Tung, R. T. Recent Advances in Schottky Barrier Concepts. *Mater. Sci. Eng., R* **2001**, *35* (1), 1-138. DOI: 10.1016/S0927-796X(01)00037-7.

(24) Brillson, L. J.; Lu, Y. ZnO Schottky Barriers and Ohmic Contacts. *J. Appl. Phys.* **2011**, *109* (12), 121301. DOI: 10.1063/1.3581173.

(25) Frost, J. C. Junction Effect Interactions in Methanol Synthesis Catalysts. *Nature* **1988**, *334* (6183), 577-580. DOI: 10.1038/334577a0.

(26) Chen, L. D.; Urushihara, M.; Chan, K.; Nørskov, J. K. Electric Field Effects in Electrochemical CO_2 Reduction. *ACS Catal.* **2016**, *6* (10), 7133-7139. DOI: 10.1021/acscatal.6b02299.

(27) Vijay, S.; Gauthier, J. A.; Heenen, H. H.; Bukas, V. J.; Kristoffersen, H. H.; Chan, K. Dipole-Field Interactions Determine the CO_2 Reduction Activity of 2D Fe–N–C Single-Atom Catalysts. *ACS Catal.* **2020**, *10* (14), 7826-7835. DOI: 10.1021/acscatal.0c01375.

(28) Sugiyama, H.; Nakamura, N.; Watanabe, S.; Kim, J.; Kitano, M.; Hosono, H. Electronic Promotion of Methanol Synthesis over Cu-Loaded ZnO-Based Catalysts. *J. Phys. Chem. Lett.* **2023**, *14* (5), 1259-1264. DOI: 10.1021/acs.jpclett.2c03427.

(29) Allen, M. W.; Weng, X.; Redwing, J. M.; Sarpatwari, K.; Mohney, S. E.; Wenckstern, H. v.; Grundmann, M.; Durbin, S. M. Temperature-Dependent Properties of Nearly Ideal ZnO Schottky Diodes. *IEEE Trans. Electron Devices* **2009**, *56* (9), 2160-2164. DOI: 10.1109/TED.2009.2026393.

(30) Chattopadhyay, P. The Effect of Shunt Resistance on the Electrical Characteristics of Schottky Barrier Diodes. *J. Phys. D: Appl. Phys.* **1996**, *29* (3), 823. DOI: 10.1088/0022-3727/29/3/047.

(31) Rahman, M. A. A Review on Semiconductors Including Applications and Temperature Effects in Semiconductors. *ASRJETS* **2014**, *7* (1), 50-70.

(32) Kuld, S.; Conradsen, C.; Moses, P. G.; Chorkendorff, I.; Sehested, J. Quantification of Zinc Atoms in a Surface Alloy on Copper in an Industrial-Type Methanol Synthesis Catalyst. *Angew. Chem., Int. Ed.* **2014**, *53* (23), 5941-5945. DOI: 10.1002/anie.201311073.

(33) Chicot, G.; Muret, P.; Santailler, J.-L.; Feuillet, G.; Pernot, J. Oxygen Vacancy and $E_C - 1$ eV Electron Trap in ZnO. *J. Phys. D: Appl. Phys.* **2014**, *47* (46), 465103. DOI: 10.1088/0022-3727/47/46/465103.

(34) Drouilly, C.; Krafft, J.-M.; Averseng, F. d. r.; Casale, S.; Bazer-Bachi, D.; Chizallet, C. l.; Lecocq, V.; Vezin, H.; Lauron-Pernot, H. l. n.; Costentin, G. n. ZnO Oxygen Vacancies Formation and Filling Followed by in Situ Photoluminescence and in Situ EPR. *J. Phys. Chem. C* **2012**, *116* (40), 21297-21307. DOI: 10.1021/jp307693y.

(35) Bosio, N.; Schaefer, A.; Grönbeck, H. Can Oxygen Vacancies in Ceria Surfaces be Measured by O1s Photoemission Spectroscopy? *J. Phys.: Condens. Matter* **2022**, *34* (17), 174004. DOI: 10.1088/1361-648X/ac4f7b.

(36) Frankcombe, T. J.; Liu, Y. Interpretation of Oxygen 1s X-ray Photoelectron Spectroscopy of ZnO. *Chem. Mater.* **2023**, *35* (14), 5468-5474. DOI: 10.1021/acs.chemmater.3c00801.

(37) Graf, A.; Isaacs, M. A.; Morgan, D. J. Insight Notes: Considerations in the XPS Analysis of O1s Spectra for Metal Oxides. *Surf. Interface Anal.* **2026**, *58* (2), 89-95. DOI: 10.1002/sia.70036.

(38) Morgan, D. J. Photoelectron Spectroscopy of Ceria: Reduction, Quantification and the Myth of the Vacancy Peak in XPS Analysis. *Surf. Interface Anal.* **2023**, *55* (11), 845-850. DOI: 10.1002/sia.7254.

(39) Posada-Borbón, A.; Bosio, N.; Grönbeck, H. On the Signatures of Oxygen Vacancies in O1s Core Level Shifts. *Surf. Sci.* **2021**, *705*, 121761. DOI: 10.1016/j.susc.2020.121761.

(40) Weichsel, C.; Pagni, O.; Leitch, A. W. R. Electrical and Hydrogen Sensing Characteristics of Pd/ZnO Schottky Diodes Grown on GaAs. *Semicond. Sci. Technol.* **2005**, *20* (8), 840. DOI: 10.1088/0268-1242/20/8/036.

(41) Doh, W. H.; Roy, P. C.; Kim, C. M. Interaction of Hydrogen with ZnO: Surface Adsorption versus Bulk Diffusion. *Langmuir* **2010**, *26* (21), 16278-16281. DOI: 10.1021/la101369r.

(42) Ip, K.; Overberg, M. E.; Heo, Y. W.; Norton, D. P.; Pearton, S. J.; Stutz, C. E.; Kucheyev, S. O.; Jagadish, C.; Williams, J. S.; Luo, B.; et al. Hydrogen Incorporation, Diffusivity and Evolution in Bulk ZnO. *Solid-State Electron.* **2003**, *47* (12), 2255-2259. DOI: 10.1016/S0038-1101(03)00207-7.

(43) Colavita, P. E.; Doescher, M. S.; Molliet, A.; Evans, Ú.; Reddic, J.; Zhou, J.; Chen, D.; Miney, P. G.; Myrick, M. L. Effects of Metal Coating on Self-Assembled Monolayers on Gold. 1. Copper on Dodecanethiol and Octadecanethiol. *Langmuir* **2002**, *18* (22), 8503-8509. DOI: 10.1021/la025941z.

(44) Thomas, D. G.; Lander, J. J. Hydrogen as a Donor in Zinc Oxide. *J. Chem. Phys.* **1956**, *25* (6), 1136-1142. DOI: 10.1063/1.1743165.

(45) Hino, J.; Tomizuka, C.; Wert, C. Internal Friction and Diffusion in 31% Alpha Brass. *Acta Metall.* **1957**, *5* (1), 41-49. DOI: 10.1016/0001-6160(57)90153-0.

(46) Christmann, K.; Ertl, G.; Pignet, T. Adsorption of Hydrogen on a Pt(111) Surface. *Surf. Sci.* **1976**, *54* (2), 365-392. DOI: 10.1016/0039-6028(76)90232-6.

(47) Kim, S.; Kang, B. S.; Ren, F.; Ip, K.; Heo, Y. W.; Norton, D. P.; Pearton, S. J. Sensitivity of Pt/ZnO Schottky Diode Characteristics to Hydrogen. *Appl. Phys. Lett.* **2004**, *84* (10), 1698-1700. DOI: 10.1063/1.1664012.

(48) Ito, K. Hydrogen-Sensitive Schottky Barrier Diodes. *Surf. Sci.* **1979**, *86*, 345-352. DOI: 10.1016/0039-6028(79)90412-6.

(49) Christensen, J. M.; Boysen, J. A.; Svensson, R.; Nielsen, N. D.; Lützen, M.; Bigom-Eriksen, L.; Fischer, J. L.; Grivel, J.-C.; Damsgaard, C. D.; Grönbeck, H.; et al. Charge Transfer Across the Metal/Oxide Interface Determines the Rate of CO_2 Hydrogenation to Methanol over Cu/ZnO Catalysts. 12 February 2026, PREPRINT (Version 1) available at Research Square. DOI: 10.21203/rs.3.rs-6939552/v1.

(50) Asadi, Z.; Marshall, C. P.; Trunschke, A.; Risse, T. Revealing the Active State of a Cu/ZnO:Al Catalyst During Reverse Water–Gas Shift Reaction in an Operando Microwave Absorption Study. *Angew. Chem., Int. Ed.* **2025**, *64* (46), e202504280. DOI: 10.1002/anie.202504280.

(51) Petersson, L. G.; Dannetun, H. M.; Lundström, I. The Water-Forming Reaction on Palladium. *Surf. Sci.* **1985**, *161* (1), 77-100. DOI: 10.1016/0039-6028(85)90729-0.

(52) Nakagomi, S.; Spetz, A. L.; Lundstrom, I.; Tobias, P. Electrical Characterization of Carbon Monoxide Sensitive High Temperature Sensor Diode Based on Catalytic Metal Gate-Insulator-Silicon Carbide Structure. *IEEE Sens. J.* **2002**, *2* (5), 379-386. DOI: 10.1109/JSEN.2002.805036.

(53) An, K.; Alayoglu, S.; Musselwhite, N.; Plamthottam, S.; Melaet, G.; Lindeman, A. E.; Somorjai, G. A. Enhanced CO Oxidation Rates at the Interface of Mesoporous Oxides and Pt Nanoparticles. *J. Am. Chem. Soc.* **2013**, *135* (44), 16689-16696. DOI: 10.1021/ja4088743.

(54) Gergen, B.; Nienhaus, H.; Weinberg, W. H.; McFarland, E. W. Chemically Induced Electronic Excitations at Metal Surfaces. *Science* **2001**, *294* (5551), 2521-2523. DOI: doi:10.1126/science.1066134.

(55) Gross, E.; Somorjai, G. A. The Impact of Electronic Charge on Catalytic Reactivity and Selectivity of Metal-Oxide Supported Metallic Nanoparticles. *Top. Catal.* **2013**, *56* (12), 1049-1058. DOI: 10.1007/s11244-013-0069-3.

(56) Hervier, A.; Renzas, J. R.; Park, J. Y.; Somorjai, G. A. Hydrogen Oxidation-Driven Hot Electron Flow Detected by Catalytic Nanodiodes. *Nano Lett.* **2009**, *9* (11), 3930-3933. DOI: 10.1021/nl9023275.

(57) Hu, Y.-S.; Kleiman-Shwarsctein, A.; Stucky, G. D.; McFarland, E. W. Improved Photoelectrochemical Performance of Ti-doped α-Fe_2O_3 Thin Films by Surface Modification with Fluoride. *Chem. Commun.* **2009**, (19), 2652-2654. DOI: 10.1039/B901135H.

(58) Ji, X.; Zuppero, A.; Gidwani, J. M.; Somorjai, G. A. The Catalytic Nanodiode: Gas Phase Catalytic Reaction Generated Electron Flow Using Nanoscale Platinum Titanium Oxide Schottky Diodes. *Nano Lett.* **2005**, *5* (4), 753-756. DOI: 10.1021/nl050241a.

(59) Ji, X. Z.; Somorjai, G. A. Continuous Hot Electron Generation in Pt/TiO_2, Pd/TiO_2, and Pt/GaN Catalytic Nanodiodes from Oxidation of Carbon Monoxide. *J. Phys. Chem. B* **2005**, *109* (47), 22530-22535. DOI: 10.1021/jp054163r.

(60) Liu, X.; Cuenya, B. R.; McFarland, E. W. A MIS Device Structure for Detection of Chemically Induced Charge Carriers. *Sens. Actuators, B* **2004**, *99* (2), 556-561. DOI: 10.1016/j.snb.2004.01.014.

(61) McFarland, E. W.; Tang, J. A Photovoltaic Device Structure Based on Internal Electron Emission. *Nature* **2003**, *421* (6923), 616-618. DOI: 10.1038/nature01316.

(62) Nienhaus, H.; Bergh, H. S.; Gergen, B.; Majumdar, A.; Weinberg, W. H.; McFarland, E. W. Selective H Atom Sensors using Ultrathin Ag/Si Schottky Diodes. *Appl. Phys. Lett.* **1999**, *74* (26), 4046-4048. DOI: 10.1063/1.123256.

(63) Park, J. Y.; Baker, L. R.; Somorjai, G. A. Role of Hot Electrons and Metal–Oxide Interfaces in Surface Chemistry and Catalytic Reactions. *Chem. Rev.* **2015**, *115* (8), 2781-2817. DOI: 10.1021/cr400311p.

(64) Park, J. Y.; Lee, H.; Renzas, J. R.; Zhang, Y.; Somorjai, G. A. Probing Hot Electron Flow Generated on Pt Nanoparticles with Au/TiO_2 Schottky Diodes during Catalytic CO Oxidation. *Nano Lett.* **2008**, *8* (8), 2388-2392. DOI: 10.1021/nl8012456.

(65) Park, J. Y.; Renzas, J. R.; Contreras, A. M.; Somorjai, G. A. The Genesis and Importance of Oxide–metal Interface Controlled Heterogeneous Catalysis; the Catalytic Nanodiode. *Top. Catal.* **2007**, *46* (1), 217-222. DOI: 10.1007/s11244-007-0331-7.

(66) Park, J. Y.; Renzas, J. R.; Hsu, B. B.; Somorjai, G. A. Interfacial and Chemical Properties of Pt/TiO_2, Pd/TiO_2, and Pt/GaN Catalytic Nanodiodes Influencing Hot Electron Flow. *J. Phys. Chem. C* **2007**, *111* (42), 15331-15336. DOI: 10.1021/jp074562h.

(67) Park, J. Y.; Somorjai, G. A. Energy Conversion from Catalytic Reaction to Hot Electron Current with Metal-semiconductor Schottky Nanodiodes. *J. Vac. Sci. Technol., B* **2006**, *24* (4), 1967-1971. DOI: 10.1116/1.2218861.

Visual Abstract